Comparative Evaluation of Some Empirical Design Techniques for CAD Optimization of Wideband U-Slot Microstrip Antennas

V. Natarajan and **D. Chatterjee**

Abstract— **In this paper three different empirical techniques, for design of wideband U-slot microstrip patch antennas on infinite, grounded substrates (ϵ_r = 1.0, 4.0, and 6.15), has been studied extensively. Methods I and III, developed by the present authors, commonly utilize the property of** *dimensional invariance* **in designing the radiating patch of the U-Slot microstrip antenna. These two methods use empirical (quadratic) curve-fit equations, and formulas for design of probe-fed rectangular patches, respectively, to initiate the corresponding probe-fed U-Slot patch designs. The second (method II) approach, published earlier by different authors, principally utilizes the distinction between four resonant frequencies and calculates the various dimensions associated with the U-Slot patch radiator. The initial U-slot designs from the three empirical techniques have been further optimized for enhanced bandwidths via: (a) parametric simulation, and (b) built-in global optimizers such as Powell and Genetic algorithms in the commercially available microstrip CAD software, IE3D. Extensive analysis, based on: (a) comparison of the three empirical design algorithms (methods I, II and III) , and, (b) impedance behavior (and VSWR characteristics) of U-slot antennas on low, medium and high permittivity substrates, show that method III is generally superior to methods I and II. Additionally, since the overall U-Slot patch dimensions follow the relation $\frac{W}{L} \approx 1.385$ (methods I and III), and, $\frac{W}{L} \approx 2.0$ (method II), U-Slot designs via methods I and III have** *lower* **cross-polar levels in the principal ($\phi = 0°, 90°$) planes compared to those obtained via method II.**

I. Introduction

Microstrip antennas are an extremely popular choice for wireless applications due to their low-profile, ease of fabrication and integration with RF circuitry [1], [2]. However, conventional probe-fed, microstrip patch configuration antennas suffer from low bandwidth characteristics. Recently, wideband impedance characteristics were achieved by properly etching a U-shaped slot on the metallic surface of the rectangular radiating patches, as in Fig. 1, on both foam [3] and microwave substrates [4]. (In this paper bandwidth of an antenna is dictated by the range of frequencies for which the return loss is $\leq$ -10 dB).

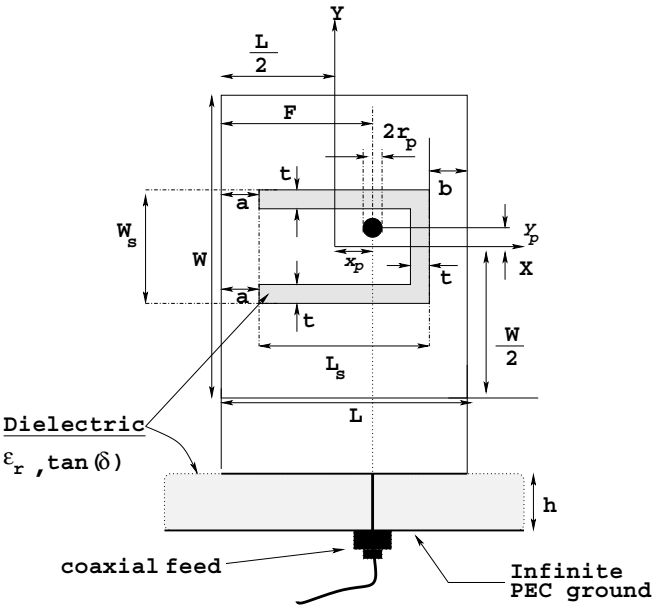

Fig. 1. Physical topology of probe-fed, wideband, U-slot microstrip antenna on microwave substrate. The dimensions shown here are independent of the coordinate system; the probe location however, is defined w.r.t the coordinate system which is located at the center of the rectangular patch. Note that the U-Slot is also located symmetrically with respect to the origin. In this paper the probe has a radius r_p and is located on the x-axis *i.e.*, $y_p = 0$, and, $F = \frac{L}{2} + x_p$ as shown here.

While no analytical models are available to describe the working of this novel U-slot microstrip antenna configuration, two different empirical methods to initiate the design of wideband U-slot antennas were presented in [5] and [6]. The subject of this investigation is to present a comparative analysis of these empirical techniques to design wideband U-slot

Department of Computer Science and Electrical Engineering, 570-F Flarsheim Hall, University of Missouri Kansas City (UMKC), 5100 Rockhill Road, KC, MO 64110, USA; e-mail:**chatd@umkc.edu**

microstrip antennas.

The empirical technique in [5] is based on dimensional invariance relationships observed in the U-slot geometry, and some empirical design equations. The design equations in [5, Section VI] were developed for specific substrate permittivities and thicknesses. The method in [6], which has been described here in subsection V. B for the sake of completeness, assumes the existence of four distinct resonant frequencies to determine the dimensions of the U-Slot. However, the applications of these equations were carried out on U-slot antenna on low permittivity (ϵ_r = 2.2) dielectrics only.

For most cases, the U-slot antenna geometries designed via the empirical techniques documented in [5] and [6] need to be further optimized, through the use of CAD tools like IE3D [7], for achieving the desired wideband impedance bandwidth behavior. The ability of these empirical techniques to generate initial U-slot antenna geometries, which can be rapidly optimized using the global optimizer sub-routines in IE3D is presented in [8]. The results indicate that the empirical technique in [5] generates initial U-slot antenna designs, which are more suitable for rapid optimization via IE3D. Extensive parametric modeling results are also presented in [5], [9] and [10] to aid designers in the selection of parameters for rapid optimization of initial U-slot antenna geometries. While the use of parametric modeling results is advocated in [6, Section V] for further optimization of the U-slot antennas, no methodology/procedure is available.

Apart from these results, the capabilities of built-in optimizers in IE3D, namely Genetic, Powell and Random algorithms, for rapid optimization and generation of wideband U-slot topologies are documented in [11]. The results reported in [11] are restricted to optimization of initial U-slot antennas designed via empirical method in [5]. A systematic approach to setting up the optimization simulations on IE3D is also described therein. The effects of dielectric permittivity and thicknesses on the performance characteristics like impedance bandwidth, gain etc., of the U-slot antennas on low, medium and high substrate permittivities are examined in [12]. These results enable a designer to select an optimal combination of substrate permittivity (ϵ_r) and thickness (h) - given a center frequency of operation (f_r) of the U-slot antenna. Such optimal selection would lead to reduced optimization cycle time.

One of the main purposes of this investigation, in addition to comparative analysis, is to present a third empirical technique for the design of wideband U-slot antennas, that is distinct from [5], [6]. A comparative analysis of the capabilities of the three empirical methods to generate initial U-slot antenna geometries, which can be rapidly optimized with minimum number of optimization cycles, is also investigated in this paper, including some appropriate case studies. To that end, parametric ([5], [9], [10]), and global optimization techniques, with the commercially available CAD software IE3D [7], are used for a comparative assesment of the three empirical design techniques.

The scope of the results presented here are restricted to probe-fed, single-layer U-slot antenna geometries on infinite grounded substrates, modeled and simulated using CAD tool IE3D. The capabilities of the global optimizers namely Genetic, and Powell optimizers are restricted to their implementations in IE3D [7]. Since optimization is an open-ended process, the procedure is stopped after achieving the desired wideband impedance characteritics. Therefore, in some cases, these designs could be modified for further enhancement of bandwidth characteristics.

The empirical equations for the resonant frequencies in [6] and [13] have been validated for low permittivity substrates in [14]. The third empirical technique (method III), described in Section III of this paper, employs the algorithm developed in [15] based on the information in [2]. The outline of the remainder of the paper is described next.

The basic problem of wideband U-slot antenna design is presented in Section II. The detailed algorithm of the proposed technique (i.e. the third empirical technique), to initiate the design of wideband U-slot antennas, is presented in Section III. The methodology followed to initiate the design of wideband U-slot antenna geometries via the different empirical techniques is outlined in Section IV. Three design examples are presented in Section V, to illustrate the abilities of the three empirical methods to initiate the design of wideband U-slot antennas. The results of simulation performance of the these initial U-slot antennas are discussed in Section VI. The step-by-step procedure used to optimize the initial U-slot antennas to achieve wideband impedance charcteristics is also described in this section. Finally, the results of the paper are summarized in Section VII, followed by the list of relevant references.

II. Problem Description

The problem associated with wideband microstrip designs as discussed in [5, Section III], concerns forming a loop in the input (Z_{in}) impedance on the

Smith chart. The loop should lie within the VSWR $\leq$ 2 circle, and most of the frequencies should be contained by the loop. All empirical techniques, followed by appropriate optimization schemes, are solely concerned in generating a U-slot design that closely satisfies this criterion.

The technique in [5, Section VII] relies on empirical design equations derived with specific substrate permittivity (ϵ_r) and thickness (h). However, it is quite impractical to derive similar equations for all possible ϵ_r and h combinations. Therefore, the applicability of these relations over all practical values of ϵ_r and design center frequency (f_r) remains very tedious.

The information gleaned from the review of [5] suggests seeking an alternate method to the design of U-slots that is much more straightforward; thus a possible alternate approach has been described in Section III.

The method in [6] is based on resonant frequency equations obtained via parametric simulations on U-slot antenna geometries on low permittivity (ϵ_r = 2.2) dielectrics. The applicability of these equations to design wideband U-slot antennas on medium and high permittivity dielectrics has not been documented. Also, the algorithm presented in [6, Section III] may generate non-physical and ambigous values for certain values of input specifications. (This aspect of the algorithm is further explored in Section V).

An empirical technique which generates the desired wideband impedance results with the least number of optimization cycles may be considered superior to others. This observation forms the basis of the comparative analysis. In this investigation, the number of optimization cycles may be characterized/identified on the basis of the following features:

- Number of optimization variables required.
- Range of optimization required in the variable.
- Optimization time.

III. An Empirical Procedure for Wideband U-Slot Antenna Design (Method III)

The empirical method in [5] relies on derived empirical formulations to obtain $\frac{W}{h}$ ratio, and the subsequent use of dimensional invariance relationships to design the U-slot antennas. As mentioned earlier, derivation of these empirical equations for every practical substrate permittivity and thickness combinations becomes quite cumbersome. The proposed empirical technique employs semi-analytical techniques [1, ch. 4], [2] to design a rectangular patch geometry, and subsequently uses the dimensional invariance relationships to design a U-shaped slot on the radiating rectangular patch.

To that end, cavity model based, custom built Fast Iterative Code (FIC) [15] is utilized to obtain the dimensions of the rectangular patch following the appropriate information in [2]. The algorithm of FIC [15] is briefly described below.

(i) Select the substrate permittivity (ϵ_r), thickness (h) and operating frequency (f_r) for the design of rectangular patch. The information presented in [14] may be used in the optimal selection of ϵ_r, h. In addition, the total number of iterations `ITMAX` is also required as input.

(ii) To account for the fringing effects, a slightly higher frequency $f_r^o \approx 1.25 f_r$ is chosen and the resonant length (L) of the radiating patch is calculated via the formula:

$$L = \frac{c}{2 f_r^o \sqrt{\epsilon_r}}. \tag{1}$$

A nominal patch width W$\approx$ 1.5$\times$L is also selected in order to facilitate the working of the FIC algorithm.

(iii) The effect of fringing fields on the resonant length of the rectangular microstrip antenna are calculated as

$$\Delta L = \frac{0.412h[\epsilon_{\mathtt{eff}}(W) + 0.3](\frac{W}{h} + 0.264)}{[\epsilon_{\mathtt{eff}}(W) - 0.258](\frac{W}{h} + 0.8)}, \tag{2}$$

where the effective relative permittivity

$$\epsilon_{\mathtt{eff}}(X) = \frac{\epsilon_r + 1}{2} + \frac{\epsilon_r - 1}{2\sqrt{1 + \frac{10h}{X}}}, \tag{3}$$

and the symbol $X \Rightarrow$ L or W, in (3).

(iv) The resonant frequency of the rectangular patch is now computed via (Hammerstad's)[1, p. 267, Eq. (4.28)]

$$f_H = \frac{c}{2(L + \Delta L)\sqrt{\epsilon_r}}, \tag{4}$$

and (James's)[1, p. 267, Eq. (4.31)]

$$f_J = \frac{f_r^o \epsilon_r}{(1 + \mathcal{X})\sqrt{\epsilon_{\mathtt{eff}}(L)\epsilon_{\mathtt{eff}}(W)}} \tag{5}$$

empirical formulas, where,

$$\begin{aligned} \mathcal{X} &= \left(\frac{h}{L}\right)\Big[0.882 + \Big(\frac{0.164(\epsilon_r - 1)}{\epsilon_r^2}\Big) \\ &+ \frac{\epsilon_r + 1}{\pi\epsilon_r}\Big(0.758 + \ln[1.88 + \frac{L}{h}]\Big)\Big]. \end{aligned} \tag{6}$$

(v) Having computed f_H and f_J the algorithm checks for the condition

$$\mathtt{min}(f_H, f_J) \leq f_r \leq \mathtt{max}(f_H, f_J). \quad (7)$$

In [2] it has been shown that the measured resonant frequency, defined by $\Im\mathrm{m}(\mathrm{Z_{in}}) = 0$, remains bounded by these two limits for low and moderate permittivity substrates. (For high permittivity substrates, resonances may not occur if the substrate thickness is too large. In that case the frequency at which the VSWR is the lowest may be considered to satisfy (7)).

(a) if the condition (7) is satisfied, the procedure stops, and resonant length L of the rectangular patch is thus found.

(b) if however, $\mathrm{f}_r < \mathtt{min}(f_H, f_J)$, then a new frequency $\mathrm{f}_r^o \Rightarrow \mathrm{f}_r^o - 0.05 \times \mathrm{f}_r$, with f_r^o given in step (ii), is selected and the procedure is repeated till the condition in (7) is satisfied.

(c) if $\mathrm{f}_r > \mathtt{max}(f_H, f_J)$, then a new frequency with $\mathrm{f}_r^o \Rightarrow \mathrm{f}_r^o + 0.05 \times \mathrm{f}_r$, with f_r^o given in step (ii), is selected and the procedure is repeated till the condition in (7) is satisfied. In the steps (a) to (c) f_r is the original operating frequency as in step (i). If the conditions (v) (a), (b) or (c) are not satisfied in the total number of iteration steps, ITMAX, then the algorithm stops.

(vi) The patch resonant length L and width W $\approx 1.5 \times$ L are obtained whenever (7) is satisfied.

The U-slot design now proceeds with the knowledge of the broader dimension W as in Fig. 1. Note that the patch resonant length, L, is redundant in the design of the U-slot. With the knowledge of W, the dimensional invariance properties [5, Section IV, Table I] are employed to obtain initial design of the U-slot.

In the process of obtaining the complete U-slot dimensions via the dimensional invariance relations, it was observed that $\frac{W}{L} \approx 1.385$, where L is the overall length of the U-slot as shown in Fig. 1, and is distinct from the length L obtained earlier for the rectangular patch from the Fast Iterative Code [15]. An alternate approach would be to apply W = 1.385 L, in step (vi) in the preceding algorithm and then obtain the complete U-slot antenna geometry via the dimensional invariance relations. However, this alternative approach is not pursued in this paper.

Having obtained the complete set of dimensions, this antenna is then modeled and simulated via commercial CAD tool IE3D (or equivalent). Based on the location and size of the impedance locus obtained on the Smith chart, the antenna geometry is further optimized for wideband performance. Note that, with the exception of the procedure used to obtain the dimensions of the width of the radiating patch, all the steps (to generate the location and dimensions of a U-shaped slot) are common to methods I and III. However, it must be emphasized that both these empirical methods produce different set of dimensions of the U-slot antennas.

The criteria $\frac{h\sqrt{\epsilon_r}}{\lambda} \approx 0.1$, 0.12, 0.14 and 0.18 [12] are used to obtain initial values of substrate permittivity (ϵ_r) and thickness (h), to design wideband U-slot antennas on air (ϵ_r = 1.0), low ($\epsilon_r \approx 2.94$), medium ($\epsilon_r \approx 4.5$) and high ($\epsilon_r \approx 9.8$) permittivity dielectrics, respectively. These choices of inputs, satisying the above criteria were observed to have small overall optimization cycles [12].

IV. Methodology

A brief description of the empirical techniques used to initiate the design of wideband U-slot antennas are presented in this section. Methods I and III essentially are based on [5] and Section III, respectively, hence are omitted here for brevity.

In [6], the effect of variation of : (a) the length of the vertical arms of the slot (L_s - t), lengths of (b) the horizontal arms of the slot (W_s), and (c) the rectangular radiating patch (L), on the resonant frequencies (assuming four distinct resonant frequencies occur) are documented for U-slot antenna on low (ϵ_r = 2.2) permittivity substrate. Based on the observation of these specific parametric modeling results, empirical equations are dervied for each of the last three resonant frequencies of the U-slot geometry. These formulas, coupled with equations in [1, ch. 4, pp. 266 - 268] to design probe-fed, rectangular microstrip antennas, are used to obtain a complete set of dimensions of U-slot antenna geometry. However, as the empirical formulas for resonant frequencies are based on parametric studies of U-slot antenna on low permittivity (ϵ_r = 2.2) dielectrics, their applicability to initiate the design of wideband U-slot antennas on other (medium or high) permittivity dielectrics remain unknown. The details of implementing the empirical design algorithm [6, Section III], and its validation, are included in Section V. B of this paper.

The wideband U-slot microstrip antenna may be considered as a structural perturbation to the classical probe-fed, rectangular microstrip patch. Therefore, once a rectangular patch antenna is designed via any

of the analytical methods in [1, ch. 4], a U-shaped slot may be etched on the surface of the radiating patch. This is the basis of a third (method III) empirical method to initiate the design of wideband U-slot antennas as presented in Section III. The location and size of the slot on the radiating patch are obtained from the dimensional invariance relations presented in [5, Section IV]. The salient features of the three empirical techniques are summarized in Table I.

TABLE I
SUMMARY OF EMPIRICAL TECHNIQUES TO INITIATE DESIGN OF WIDEBAND U-SLOT MICROSTRIP ANTENNAS

Method	Basic Concepts & Features	Reference	Inputs Required
I	Empirical design equations to calculate $\frac{W}{h}$ ratio and dimensional invariance relations.	[5]	ϵ_r, h, f_r
II	Empirically derived resonant frequency formula of the U-slot geometry and rectangular microstrip antenna design equations in [1, ch. 4, pp. 266 to 268]	[6]	ϵ_r, h, f_r, % bandwidth, $\frac{(L_s-t)}{W}$ ratio
III	Design rectangular patch microstrip antenna via analytical models in [1, ch. 4]. A U-shaped slot is cut on the surface of the radiating patch using dimensional invariance relations [5]	Section III, this paper	ϵ_r, h, f_r

The initial U-slot antenna geometries obtained from the three empirical techniques may require further optimization to yield wideband impedance behavior. These initial U-slot antennas are modeled and simulated assuming infinite, grounded dielectrics via IE3D [7]. Based on the impedance behavior of each of these initial U-slot topologies, they were optimized for further bandwidth enhancement. The optimization of these initial U-slot antennas designed via the three empirical techniques were carried out by the following two approaches.

(a) Use of parametric simulation results in [5, Section V], [9] and [10] in the selection of optimization parameters, and subsequent variation of these parameters to generate wideband impedance behavior.

(b) Selection of optimization variables based on the parametric modeling results in [5, Section V], [9] and [10] and use of global optimizers in commercial CAD tool IE3D, namely Genetic, Random and Powell optimizers [7] to generate wideband radiators.

The immediately preceding steps (a) and (b) together form the central part of this investigation as presented in this paper. Results corresponding to steps (a) and (b) are included in Sections VI A and B, respectively.

The ability of the three empirical methods to generate initial U-slot antenna geometries, which can be rapidly optimized via these two approaches is illustrated with some design examples in the ensuing section.

V. CASE STUDIES AND DESIGN ISSUES

This section documents the capabilities and limitations of the three empirical methods to initiate the design of wideband U-slot antennas, via the following design examples.

- Design Example (a): ϵ_r = 1.0 and f_r = 0.9 GHz
- Design Example (b): ϵ_r = 4.0 and f_r = 3.26 GHz
- Design Example (c): ϵ_r = 6.15 and f_r = 2.4 GHz

In all the three examples U-slot antennas exhibiting 2:1 VSWR bandwidths $\geq$ 20% are considered wideband radiators.

A. Design Using Methods I and III

Applying the criteria $\frac{h\sqrt{\epsilon_r}}{\lambda} \approx 0.10$, 0.14 and 0.16 [12], substrate thicknesses (h) of 33.31 mm, 6.45 mm and 7.56 mm were chosen to initiate the design of U-slot antennas, for design examples (a), (b) and (c), via empirical method in [5] (or method I). Here λ corresponds to the respective design frequencies (f_r) of the design examples. Since no formulations exist to initiate the design of U-slot antennas for design example (a) via method I at h = 33.31 mm, the empirical equations derived for ϵ_r = 1.0 and h = 18.0 mm [5, Table II] were used to obtain the $\frac{W}{h}$ ratio. As indicated earlier, this is one of the difficulties of method in [5]. Similarly, empirical equations derived for ϵ_r = 4.5 and h = 6.35 mm and ϵ_r = 4.5 and h = 10.0 mm were used to calculate the $\frac{W}{h}$ ratios for design examples (b) and (c), respectively. The remaining dimensions of the U-slot antenna geometries for the three design examples were calculated following the procedure documented in [5, Section VII].

For U-slot antennas designed via method III, criteria similar to those used for method I were used to select the values of substrate thicknesses (h). The cavity model based FIC and dimensional invariance relations were then used to obtain the dimensions of a rectangular patch and U-shaped slot, respectively.

B. Design Using Method II

The algorithm for the empirical design method in [6, Section III] (or method II), is described here including its implementation and validation. The description is necessary for a comparative analysis of the three methods, later in this paper.

The algorithm assumes existence of four distinct resonant frequencies for the U-Slot patch antenna, f_{res1}, f_{res2}, f_{res3} and f_{res4}. Before presenting the algorithm, the various physical distinctions associated with the resonant frequencies are identified following their original description in [6].

- f_{res1} is associated with the resonance of the slot embedded in the microwave substrate
- f_{res2} is related to the resonance of the TM_{01} mode of the patch
- f_{res3} is dependent in a complex manner with the x- and y-directed patch resonant modes
- f_{res4} can be related to the resonance of the slot in air including the effects of the "pseudopatch" that is formed inside the U-Slot

Since no analytical theory is presented in [6], one simply cannot be assured of the validity of these distinctions. In addition, for electrically "thick" substrates the existence of distinct resonant frequencies is not always possible. However, it is also known from the basic theory of microstrip antennas that an increase in the electrical thickness ($\frac{h\sqrt{\epsilon_r}}{\lambda}$) of the substrate increases the impedance bandwidth [1, p. 288, Fig. 4.16]. This observation suggests that the design technique in [6] may work well only for electrically thin substrates. Consequently, one may expect that the initial design of the U-Slot via [6] would exhibit lower impedance bandwiths and hence would need to undergo significant optimization cycles using the CAD tool IE3D [7]. One of the major purposes of this study is to investigate, via several case studies, if the initial U-Slot design via [6] (or method II) is indeed relatively difficult to optimize as compared to the initial designs via methods I [5], and III. The sequence of steps of the design algorithm from [6, Section III] are summarized next. (The dimensions are as shown in Fig. 1.)

Step 1: The algorithm requires the following inputs: (a) f_{res3}, (b) 10 dB return loss bandwidth ($\frac{\Delta f}{\mathrm{f}_{res3}}$) in %, (c) the ratio $\frac{\mathrm{L}_s-\mathrm{t}}{\mathrm{W}}$. One then calculates

$$\mathrm{f}_{res2} = \mathrm{f}_{res3} - \frac{\Delta f}{2} \times 100, \tag{8}$$

and,

$$\mathrm{f}_{res4} = \mathrm{f}_{res3} + \frac{\Delta f}{2} \times 100, \tag{9}$$

respectively.

Step 2: The substrate thickness (h) and permittivity (ϵ_r) are chosen to satisfy

$$\mathrm{h} \geq 0.06 \frac{\lambda_{res3}(\mathrm{air})}{\sqrt{\epsilon_r}}. \tag{10}$$

In (10) $\lambda_{res3}(\mathrm{air}) = \frac{v_\circ}{\mathrm{f}_{res3}}$ is the free-space wavelength corresponding to the frequency f_{res3}, and $v_\circ = 2.997925 \times 10^{+10}$ cms/sec is the velocity of electromagnetic waves in free-space.

Step 3: The overall resonant length (Fig. 1) of the patch plus the extensions due to fringe effects, is given by

$$\mathrm{L} + 2\Delta\mathrm{L} \approx \frac{v_\circ}{2\sqrt{\epsilon_r}\mathrm{f}_{res3}}. \tag{11}$$

Step 4: The overall width of the patch is given by $\mathrm{W} = 1.5 \times (\mathrm{L} + 2\Delta\mathrm{L})$.

Step 5: The overall effective permittivity and the patch resonant length extension are calculated separately as,

$$\epsilon_{\mathtt{eff}} = \frac{\epsilon_r + 1}{2} + \frac{\epsilon_r - 1}{2}\left(1 + \frac{12\mathrm{h}}{W}\right)^{-\frac{1}{2}}, \tag{12}$$

and,

$$2\Delta\mathrm{L} = 0.824\mathrm{h}\frac{(\epsilon_{\mathtt{eff}} + 0.3)(\frac{\mathrm{W}}{h} + 0.262)}{(\epsilon_{\mathtt{eff}} - 0.258)(\frac{\mathrm{W}}{h} + 0.813)}. \tag{13}$$

Interestingly, (12) and (13) are closely similar and identital to equations (3) and (2), respectively.

Step 6: The overall patch resonant length is now re-calculated as

$$\mathrm{L} = \frac{v_\circ}{2\sqrt{\epsilon_{\mathtt{eff}}}\mathrm{f}_{res3}} - 2\Delta\mathrm{L}. \tag{14}$$

Step 7: The slot thickness, t, is calculated via the relationship

$$\mathrm{t} = \frac{\lambda_{res3}(\mathrm{air})}{60}. \tag{15}$$

Step 8: Calculate the slot width

$$\mathrm{W_s} = \frac{v_\circ}{\sqrt{\epsilon_{\mathtt{eff}}}\mathrm{f}_{res2}} - 2(\mathrm{L} + 2\Delta\mathrm{L} - t). \tag{16}$$

Step 9: Select L_s such that

$$\frac{\mathrm{L}_s - t}{\mathrm{W}} \geq 0.3 \text{ and } \frac{\mathrm{L}_s - t}{\mathrm{W_s}} \geq 0.75. \tag{17}$$

Step 10: Calculate the effective permittivity and the length extension of the "pseudopatch" as

$$\epsilon_{\mathtt{eff}(\mathrm{pp})} = \frac{\epsilon_r + 1}{2} + \frac{\epsilon_r - 1}{2}\left(1 + \frac{12\mathrm{h}}{\mathrm{W}_s - 2t}\right)^{-\frac{1}{2}}, \tag{18}$$

and,

$$2\overline{\Delta}_{\rm pp} = 0.824{\rm h}\frac{(\epsilon_{\tt eff(pp)}+0.3)(\frac{{\rm W}_s-2t}{h}+0.262)}{(\epsilon_{\tt eff(pp)}-0.258)(\frac{{\rm W}_s-2t}{h}+0.813)}. \quad (19)$$

Step 11: The quantity

$$\begin{aligned} {\rm b} &\approx {\rm L}-t+2\overline{\Delta}_{\rm pp}-\frac{1}{\sqrt{\epsilon_{\tt eff(pp)}}} \\ &\times \left(\frac{v_\circ}{{\rm f}_{res4}}-\{2({\rm L}_s-t)+{\rm W}_s\}\right). \quad (20) \end{aligned}$$

Step 12: The algorithm checks the condition

$$({\rm L}_s+{\rm b}) \leq {\rm L}.$$

If this condition is not satisfied, one adjusts the quantity $({\rm L}_s-t)$ step # 9 and keeps recalculating b in step # 11, till the condition in step # 12 is satisfied and a physically realizable design for the U-Slot microstrip patch antenna is feasible.

The implementation of the above algorithm was validated for the design of the U-Slot dimensions of $\epsilon_r = 2.2$ and ${\rm h} = 0.635$ cms at ${\rm f}_{res3} = 2.15$ GHz, as available in [6, Table IV]. However, when the algorithm of method II was subsequentlly applied to the calculation of the initial U-Slot dimensions for $\epsilon_r = 4.0$ and 6.15, one of the dimensions turned out non-physical. The details are included in Table II, below.

TABLE II
NON-PHYSICAL OUTPUTS OBTAINED VIA METHOD II ([6]), REFERRING TO FIG. 1. (ALL DIMENSIONS IN MM)

Parameter; (Type: Input/Output)	Example (b)	Example (c)
ϵ_r (input)	4.0	6.15
h (input)	6.45	7
$\frac{\Delta {\rm f}}{{\rm f}_{res3}}$(% bandwidth); (input)	25	30
${\rm f}_{res3}$ in GHz;(input)	3.26	2.4
$\frac{({\rm L}_s-t)}{\rm W}$; (input)	0.4	0.4
W; (output)	34.49	37.78
L; (output)	17.15	19.18
${\rm L}_s$; (output)	15.33	15.11
${\rm W}_s$; (output)	14.66	19.46
t; (output)	1.53	2.08
b; (output)	-2.0018	-5.1102
Comment	b $<$ 0.0 (*non-physical*)	b $<$ 0.0 (*non-physical*)

At this stage, in view of the results in Table II, it appears appropriate that a comparative analysis of the three methods be presented. This, expectedly, would help in understanding the salient features of method II and its standing with respect to methods I and III.

Following [5], application of methods I and III is initiated by the combination of substrate parameters, satisfying the criterion $\frac{{\rm h}\sqrt{\epsilon_r}}{\lambda} \approx 0.14$ for low and medium permittivities. (For substrates with $\epsilon_r \geq 6.0$ a value of 0.18 was found to yield acceptable results [5]). Beyond this point, methods I and III differ noticeably and their intrinsic differences are briefly summarized below.

For method I, assuming the substrate geometry is known uniquely, empirical equations [5, Table II] are used. (For situations where there exists no empirical equations corresponding exactly to the particular substrate type, an 'average' design procedure is adopted as explained in detail in [5, Section VII]). The main purpose of method I, however, is to obtain the appropriate $\frac{\rm W}{\rm h}$ ratio from the empirical equations. Knowing the substrate thickness, h, one readily calculates the overall U-Slot patch width W for a typical ϵ_r and design/operating frequency, ${\rm f}_r$. Once W is known, the other dimensions of the U-Slot can be calculated very quickly by using the dimensional invariance relationships as in [5, Table I]. The rapid calculation of the dimensions essentially resembles the back-of-the-envelope process. The main disadvantage of method I, however, is that the starting empirical equations are available for a few select substrate cases, and hence the accuracy of the average design procedures are questionable. For greater accuracy, one needs to derive empirical equations for a given combination of ϵ_r and h, which in itself can be very tedious.

The preceding limitation of method I is circumvented by the algorithm of method III, described in Section III. With the knowledge of the substrate geometry and the design frequency, one can determine the larger patch width, W, via eqs. (1) to (7). Once W is known, regardless of the $\frac{\rm W}{\rm h}$ ratio, the dimensional invariance relationships from [5, Table I] can be used to complete the U-Slot radiating patch design, just as in method I. The primary advantage of this approach, over method I, is that equations (1) to (7) apply to an arbitrary class of substrate topologies, as long as the assumptions of the cavity-model remains valid in that particular case. (In [2] it has been shown that these cavity-model formulas are applicable to $\epsilon_r \approx 12.0$.) Thus even for substrates where the empirical equations (method I) are not directly available, one can still proceed to design a U-Slot by first obtaining the overall rectangular patch dimensions (method III). Since the theoretical validity of these cavity-model formulas is well-known [1], [2], method III is far more

versatile and expected to be accurate than method I.

Method II in [6], as discussed here, has some inherent limitations in its applications. The two initial U-Slot patch designs for $\epsilon_r = 4.0$ and 6.15, as shown in Table II, could yield non-physical dimensions, b, (Fig. 1). Incidentally, one notes that from a numerical standpoint the condition in step 12 is still satisfied even with the negative value of the b dimension in Fig. 1. In absence of a comprehensive analytical theory for the U-Slot, this apparent limitation for method II was investigated as explained below.

Since the initial design [6] for the U-Slot relies on the existence of distinct resonant frequencies, it maybe hypothesized that the design algorithm would be physically viable if the parameter $\frac{\mathrm{h}\sqrt{\epsilon_r}}{\lambda_{\mathrm{res3}}(\mathrm{air})}$ is small. For the two cases listed in Table II, one finds $\frac{\mathrm{h}\sqrt{\epsilon_r}}{\lambda_{\mathrm{res3}}(\mathrm{air})} \approx 0.09$ and 0.125 for $\epsilon_r = 4.0$ and 6.15, respectively. The exact nature of dependence of b on the substrate permittivity ϵ_r and thickness h is complicated, because of the nature of the algebraic forms of the various intermediate quantities as appearing in equations (12) to (20). Preliminary examination of (20) indicates that for $\mathrm{b} > 0$, (physically realizable geometry), the additional condition

$$\mathrm{L} - \mathrm{t} + 2\overline{\Delta}_{\mathrm{pp}} \gg \frac{1}{\sqrt{\epsilon_{\mathtt{eff}}(\mathrm{pp})}}\left[\frac{\mathrm{v}_\circ}{\mathrm{f}_{res4}} - 3.5\mathrm{W_s}\right] \quad (21)$$

needs to be satisfied. (Condition (21) easily follows from the second condition in (17), and (20)). From the present investigations, it appears that (21) is generally satisfied when $\frac{\mathrm{h}\sqrt{\epsilon_r}}{\lambda_{\mathrm{res3}}(\mathrm{air})} \leq 0.075$. Consequently, in light of the current analysis, it appears that the condition (10) in step 2 could be modified to read:

$$0.06 \leq \frac{\mathrm{h}\sqrt{\epsilon_r}}{\lambda_{\mathrm{res3}}(\mathrm{air})} \leq 0.075. \quad (22)$$

This implies that physically valid initial U-Slot patch designs following the algorithm in [6] are feasible for low permittivity substrates. This observation has the further impact that these initial designs via [6] could exhibit low, 10 dB return loss bandwidths. Hence, these initial designs obtained from method II (or [6]), when subjected to parametric or global optimization schemes via commercial CAD softwares such as IE3D [7], would require increased optimization cycles (as defined in Section II).

However, it is emphasized that this aspect of implementing the algorithm in [6] needs to be investigated in more detail, before the condition (22) could be considered acceptable.

The dimensions of the U-slot antennas obtained via the three methods for design examples (a), (b) and (c) are tabulated in Tables III, IV and V, respectively. The U-slot antenna geometries obtained via methods I, II and III, for the three design examples, were modeled and simulated assuming infinite grounded dielectrics via commercial CAD tool IE3D [7]. Based on the location and size of the impedance locus on the Smith chart, optimization parameters were chosen for subsequent optimization of the initial U-slot antenna geometries. The analysis of the results are discussed in the following section.

VI. Results and Discussion

The results of the performed simulations, and the subsequent optimization of the initial U-slot antennas designed via the three empirical methods, are discussed in details in this section. To that end, the results obtained via the use of parametric simulation results in [5], [9] and [10] are discussed next in part A, followed by results obtained via `IE3D` global optimizers in part B. In addition, boresight gain vs. frequency, and principal plane ($\phi = 0^\circ$ and 90°) co- and cross-polar radiation patterns, for initial and optimized U-Slot patch geometries (for $\epsilon_r = 4.0$ in Table IV), are also included in part C for a complete understanding of the antenna performance. A comparative performance analysis of the three empirical design techniques, based on bandwidth, gain and radiation characteristics, is presented in part D.

A. Optimization via Parametric Modeling Results in [5], [9] and [10]

The results of U-slot antennas, designed via the three empirical techniques and further optimization via parametric modeling results are shown in Figs. 2 to 14. The impedance loci of the U-slot antennas obtained from the three empirical methods for design example (a) are shown in Fig. 2. From the Smith chart results, U-slot antennas designed via methods I and III form impedance loops close to the center of the Smith chart. In contrast, the U-slot antenna from method II appears to be highly capacitive, with its impedance loop on the lower half and farthest from the center of the Smith Chart.

The impedance loci of the (final) optimized U-slot antenna geometries obtained from methods I, II and III, for design example (a), are shown in Fig. 3. All three optimized U-slot antennas appear to exhibit wideband impedance behavior.

The results of the initial and optimized U-slot antennas designed via the three empirical techniques, for examples (b) and (c), are in Figs. 4 to 8. The

TABLE III
DIMENSIONS OF INITIAL AND OPTIMIZED, (VIA PARAMETRIC MODELING RESULTS IN [5], [9], [10]) U-SLOT ANTENNAS OBTAINED VIA THE THREE EMPIRICAL METHODS FOR DESIGN EXAMPLE (A), REFERRING TO FIG. 1. (ALL DIMENSIONS IN MM)

Parameter	Method I		Method II		Method III	
	Initial	Optimized	Initial	Optimized	Initial	Optimized
ϵ_r	1.0	1.0	1.0	1.0	1.0	1.0
$\tan(\delta)$	0.0	0.0	0.0	0.0	0.0	0.0
h	33.31	33.31	25.0	25.0	33.31	33.31
L	159.24	159.24	131.56	131.56	129.42	129.42
W	220.38	220.38	249.83	249.83	178.85	178.85
L_s	110.24	110.24	80.45	80.45	89.46	89.46
W_s	85.65	85.65	48.12	55.0	69.51	69.51
t	12.33	12.33	5.55	5.55	10.01	10.01
a	24.5	24.5	2.99	2.99	19.98	19.98
b	24.5	24.5	48.12	48.12	19.98	19.98
F	79.62	83.62	65.78	65.78	64.71	66.71
R_{probe}	3.0	4.0	2.0	2.0	3.0	3.5

TABLE IV
DIMENSIONS OF INITIAL AND OPTIMIZED, (VIA PARAMETRIC MODELING RESULTS IN [5], [9], [10]) U-SLOT ANTENNAS OBTAINED VIA THE THREE EMPIRICAL METHODS FOR DESIGN EXAMPLE (B), REFERRING TO FIG. 1. (ALL DIMENSIONS IN MM)

Parameter	Method I		Method II		Method III	
	Initial	Optimized	Initial	Optimized	Initial	Optimized
ϵ_r	4.0	4.0	4.0	4.0	4.0	4.0
$\tan(\delta)$	0.002	0.002	0.002	0.002	0.002	0.002
h	6.45	6.45	5.5	5.5	6.45	6.45
L	21.18	21.18	17.96	17.96	18.44	18.44
W	29.32	29.32	34.49	34.49	25.54	25.54
L_s	14.66	14.66	16.01	13.53	12.76	12.76
W_s	11.39	11.39	15.94	12.0	9.93	9.93
t	1.64	1.64	1.53	1.53	1.43	1.43
a	3.76	3.76	0.95	2.43	2.84	2.84
b	3.76	3.76	1.0	2.0	2.84	2.84
F	10.59	9.59	8.96	8.96	9.22	7.72
R_{probe}	0.635	0.635	0.635	0.635	0.635	0.635

TABLE V
DIMENSIONS OF INITIAL AND OPTIMIZED, (VIA PARAMETRIC MODELING RESULTS IN [5], [9], [10]) U-SLOT ANTENNAS OBTAINED VIA THE THREE EMPIRICAL METHODS FOR DESIGN EXAMPLE (C), REFERRING TO FIG. 1. (ALL DIMENSIONS IN MM)

Parameter	Method I		Method II		Method III	
	Initial	Optimized	Initial	Optimized	Initial	Optimized
ϵ_r	6.15	6.15	6.15	6.15	6.15	6.15
$\tan(\delta)$	0.002	0.002	0.002	0.002	0.002	0.002
h	7.56	7.56	3.1	7.0	7.56	7.56
L	21.06	21.06	22.42	22.42	20.22	20.22
W	29.14	29.14	37.78	37.78	27.98	27.98
L_s	14.58	14.58	21.35	17.35	14.0	14.0
W_s	11.53	11.53	18.89	14.89	10.87	10.87
t	1.63	1.63	2.08	2.08	1.57	1.57
a	3.24	3.24	0.16	2.16	3.11	3.11
b	3.24	3.24	0.95	2.95	3.11	3.11
F	10.53	8.03	11.21	11.23	10.11	7.61
R_{probe}	0.635	0.635	0.635	0.635	0.635	0.635

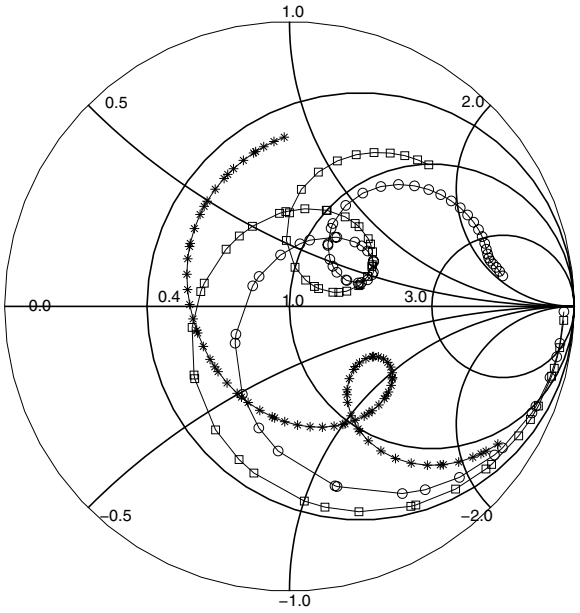

Fig. 2. Comparison of impedance loci of initial U-slot antennas from the three empirical methods for design on dielectric substrates with $\epsilon_r = 1.0$ via IE3D [7]; $\square - \square - \square$- method I; $* - * - *$- method II; $\circ - \circ - \circ$-method III.

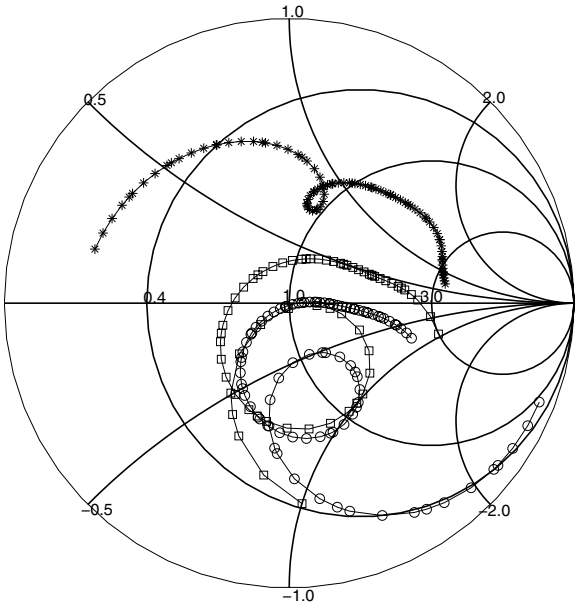

Fig. 4. Comparison of Smith Chart results of initial U-slot antennas from the three empirical methods on dielectric substrates with $\epsilon_r = 4.0$ via IE3D [7]; $\square - \square - \square$- method I; $* - * - *$- method II; $\circ - \circ - \circ$- method III.

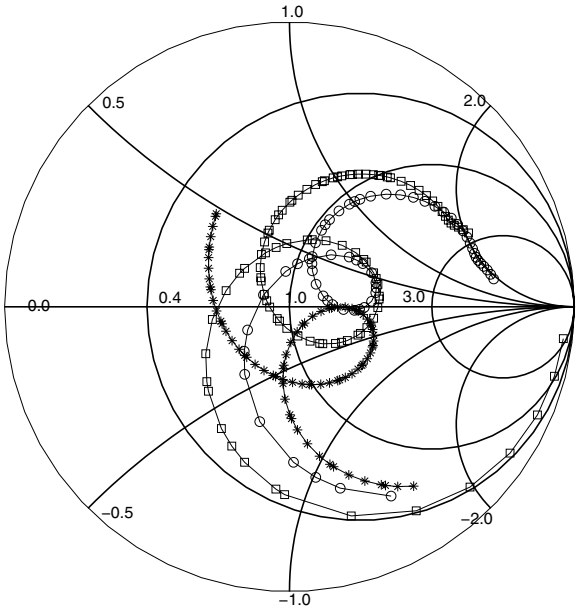

Fig. 3. Comparison of impedance loci of final, optimized U-slot antennas from the three empirical methods on dielectric substrates with $\epsilon_r = 1.0$ via IE3D [7]; $\square - \square - \square$- method I; $* - * - *$- method II; $\circ - \circ - \circ$- method III.

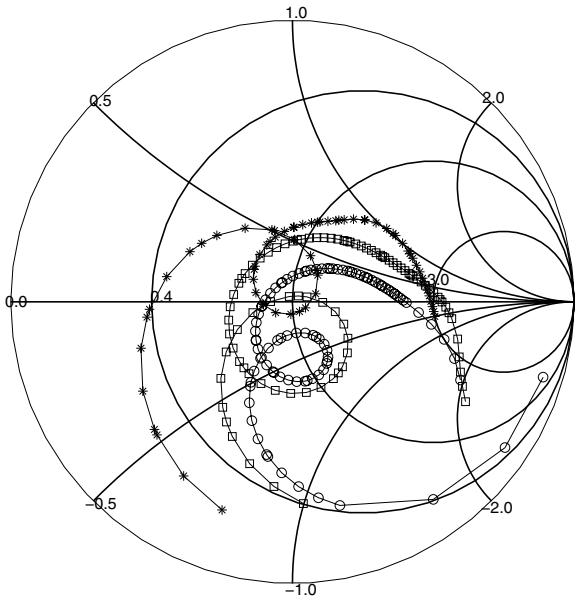

Fig. 5. Comparison of Smith Chart results of final, optimized U-slot antennas from the three empirical methods on dielectric substrates with $\epsilon_r = 4.0$ via IE3D [7]; $\square - \square - \square$-method I; $* - * - *$- method II; $\circ - \circ - \circ$- method III.

impedance behavior of the initial U-slot antenna designs on ϵ_r = 4.0 (Fig. 4) and ϵ_r = 6.15 (Fig. 7) show that the design via method II, for examples (b) and (c), do not form loops close to the center of the Smith Chart, in contrast with methods I and III. Following parametric modeling results in [5], [9] and [10], these U-slot antennas were optimized for wideband impedance characteristics, as shown in Figs. 5 to 6 for example (b), and Fig. 8 for example (c), respectively. In both cases, the final optimized impedances loci form loops in the VSWR ≤ 2 region of the Smith chart.

The choice of the optimization parameters (such as

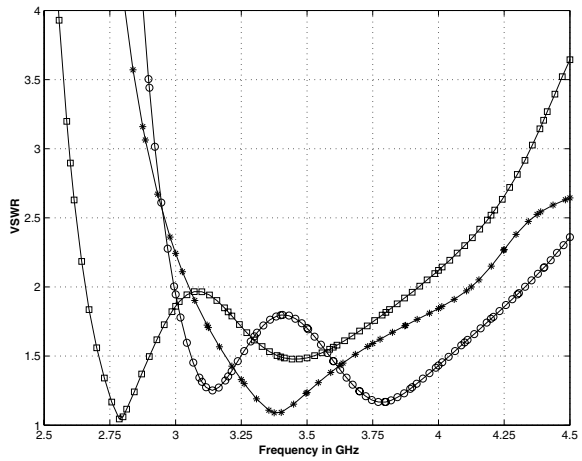

Fig. 6. Comparison of VSWR results of final, optimized U-slot antennas from the three empirical methods on dielectric substrates with $\epsilon_r = 4.0$ via IE3D [7]; $\square - \square - \square$- method I; $* - * - *$- method II; $\circ - \circ - \circ$- method III.

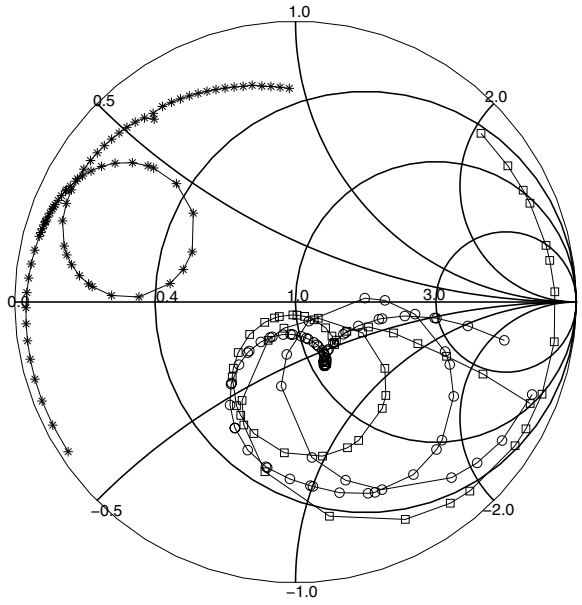

Fig. 7. Comparison of Smith Chart results of initial U-slot antennas from the three empirical methods on dielectric substrates with $\epsilon_r = 6.15$ via IE3D [7]; $\square - \square - \square$- method I; $* - * - *$- method II; $\circ - \circ - \circ$- method III.

width of slot, length of slot, probe location etc.), is based on the size and location of the impedace loci of the initial U-slot antennas on the Smith chart, and the knowledge of the parametric simulations results documented in [5], [9] and [10].

To that end, probe location and radii were chosen as optimization variables for U-slot antennas for example (a), designed via methods I and III. In contrast, for the U-slot antenna designed via method II, the length of the horizontal arm (W_s) was chosen as the optimization variables.

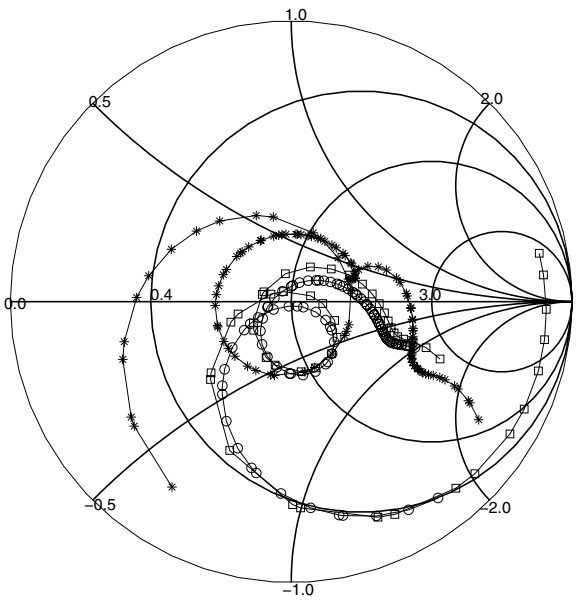

Fig. 8. Comparison of Smith Chart results of final, optimized U-slot antennas from the three empirical methods on dielectric substrates with $\epsilon_r = 6.15$ via IE3D [7]; $\square - \square - \square$-method I; $* - * - *$-method II; $\circ - \circ - \circ$- method III.

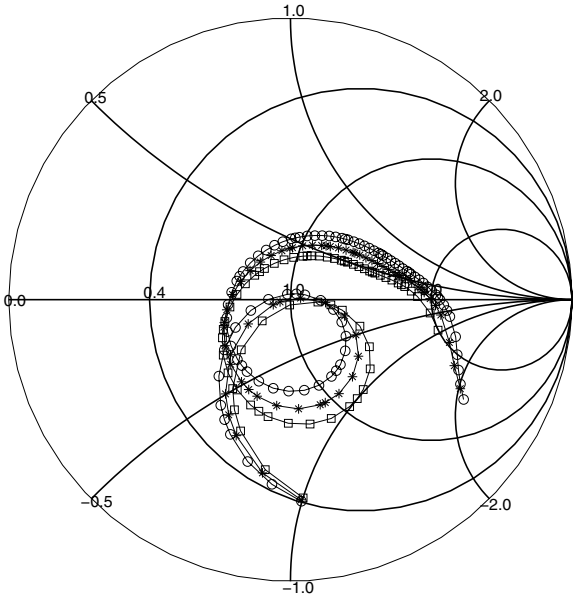

Fig. 9. Optimization Process for U-slot antenna designed via method I on dielectric substrates with $\epsilon_r = 4.0$ using parametric modeling results in [5], [9] and [10]; $\square - \square - \square$- Initial, unoptimized; X_p = 0.0, Y_p = 0.0; $* - * - *$- X_p = 0.0, Y_p = 0.5; $\circ - \circ - \circ -$ X_p = 0.0, Y_p = 1.0; all other dimensions of the U-slot antenna are kept constant - all dimensions in mm.

It is interesting to note (from Table III) that, while, methods I and III require two optimization variables to produce wideband bandwidth characteristics, the range of variation of each of these optimization variable is quite small. In comparison, method II requires

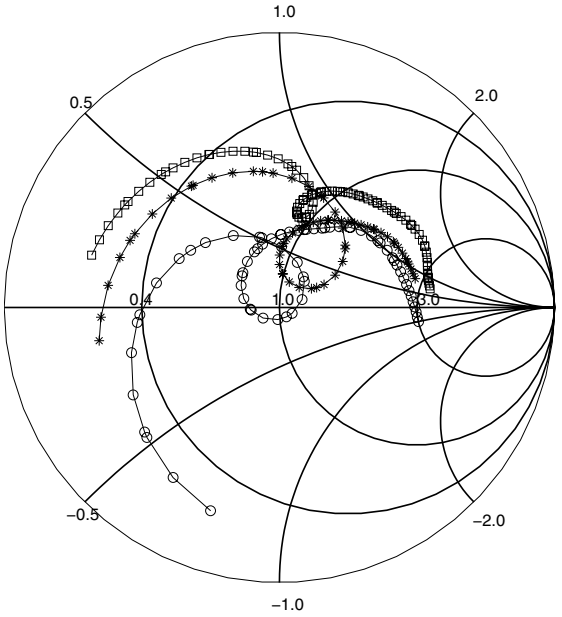

Fig. 10. Optimization Process for U-slot antenna designed via method II on dielectric substrates with ϵ_r = 4.0 using parametric modeling results in [5], [9] and [10]; □ − □ − □- Initial, unoptimized; L_s = 16.01, W_s = 15.94, a = 0.95 and b = 1.0; ∗ − ∗ − ∗- Step1 -L_s = 12.0, W_s = 15.94, a = 2.43 and b = 2.0; ○ − ○ − ○− Step2 - L_s = 12.0, W_s = 13.0, a = 2.43 and b = 2.0; all other dimensions of the U-slot antenna are kept constant - all dimensions in mm.

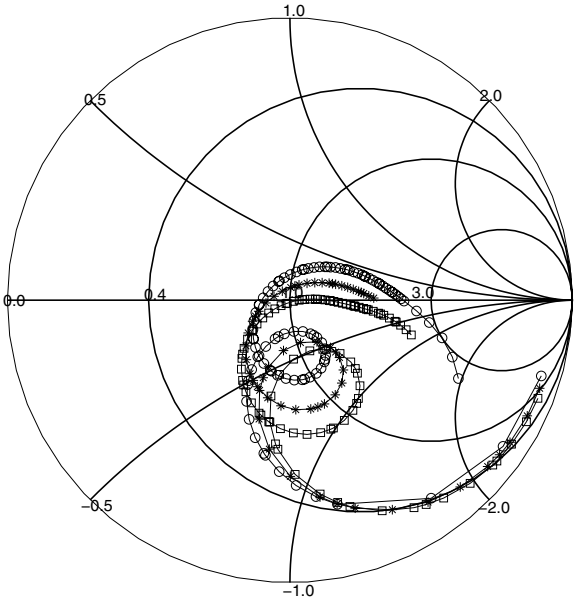

Fig. 11. Optimization Process for U-slot antenna designed via method III on dielectric substrates with ϵ_r = 4.0 using parametric modeling results in [5], [9] and [10]; □ − □ − □- Initial, unoptimized; X_p = 0.0, Y_p = 0.0; ∗ − ∗ − ∗- X_p = 0.0, Y_p = 0.75; ○ − ○ − ○− X_p = 0.0, Y_p = 1.5; all other dimensions of the U-slot antenna are kept constant - all dimensions in mm.

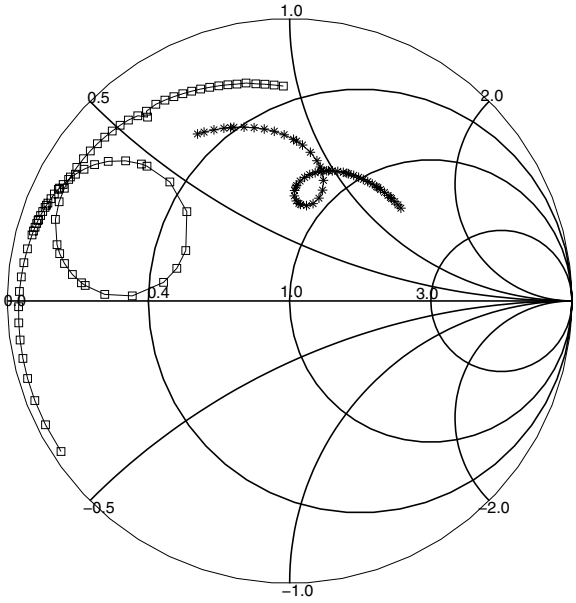

Fig. 12. Optimization Process for U-slot antenna designed on dielectric substrates with ϵ_r = 6.15 via method II; □ − □ − □- Initial; h = 3.1; ∗ − ∗ − ∗- h = 7.0; all other dimensions of the U-slot antenna are kept constant - all dimensions in mm.

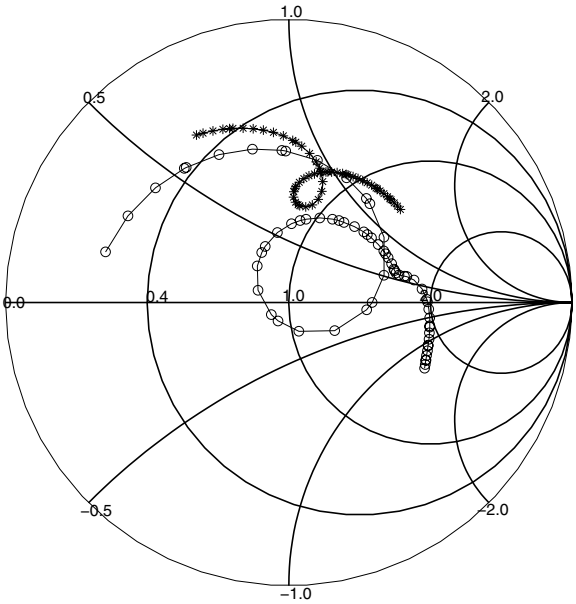

Fig. 13. Optimization Process for U-slot antenna designed on dielectric substrates with ϵ_r = 6.15 via method II; ∗ − ∗ − ∗- h = 7.0, L_s = 21.35, a = 0.6 and b = 0.95; ○ − ○ − ○- h = 7.0, L_s = 17.35, a = 2.16 and b = 2.95; all other dimensions of the U-slot antenna are kept constant - all dimensions in mm.

only one optimization variable. However, the range of variation required to achieve wideband impedance characteristics is quite large (W_s - from 48.12 mm to 55.0 mm). This may increase the optimization time and hence the optimization cycle for method II in comparison with methods I and III.

For design example (b), the initial U-slot antennas obtained from both methods I and III, form impedance

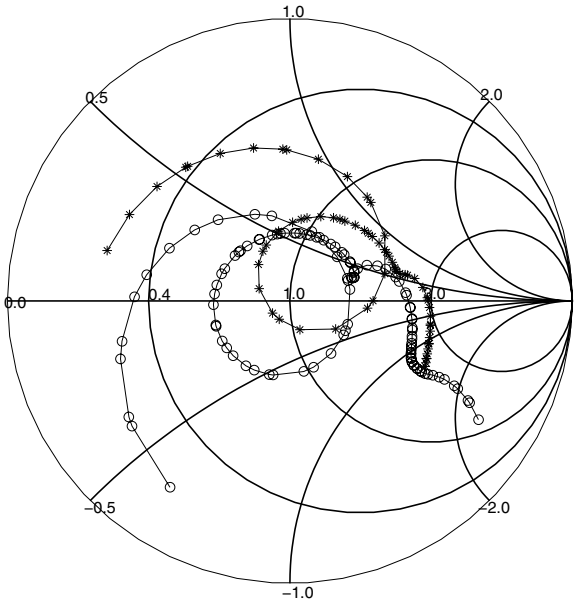

Fig. 14. Optimization Process for U-slot antenna designed on dielectric substrates with ϵ_r = 6.15 via method II; $*-*-*-*$- h = 7.0, L_s = 17.35, a = 2.16, b = 2.95 and $W_s = 18.89$; $\circ-\circ-\circ-\circ$- Optimized- h = 7.0, L_s = 17.35, a = 2.16, b = 2.95 and W_s = 14.89; all other dimensions of the U-slot antenna are kept constant - all dimensions in cms.

loops very close to the center of the Smith chart (Fig. 4). Therefore, only their probe locations were varied to obtain wideband impedance characteristics as evident from Figs. 9 and 11, respectively. In contrast, the U-slot antenna designed via method II does not form an impedance loop close to the center of the Smith chart. (Fig. 4). Hence, multi-step (multi-parameter) optimizations must be pursued to achieve wideband impedance characteristics. The multi-parameter/multi-step optimization procedure is shown in Fig. 10.

As seen in Fig. 10, in step 1, the length of the vertical arms of the U-slot are varied from 16.01 mm to 11.53 mm. This optimization moves the impedance loop closer to the center of the Smith chart. Then, the width of the horizontal arm (W_s) is chosen as the optimization variable in step 2 to shift the impedance locus within the 2:1 VSWR circle.

A similar feature is observed in the optimization procedure for U-slot antennas for example (c) via the three empirical methods. For U-slot antennas designed via methods I and III, the location of the probe feed is chosen as optimization variable. The optimization procedure of U-slot antennas designed via methods I and III are similar to those shown in Figs. 9 and 11, and are omitted here for brevity. In contrast, substrate thickness (h), width of the horizontal arm (W_s) of the U-slot and lengths of the arms (L_s) were chosen as optimization variables for U-slot antennas designed via method II. The step-by-step optimization procedure is documented in Figs. 12 to 14.

In the first step of the optimization process, (in Fig. 12), the substrate thickness of the U-slot antenna is increased from h = 3.1m to 7.0 mm, shifting the impedance locus closer to the center of the Smith Chart. Then, in the second step, the length of the arms of the slot (L_s) are reduced, as shown in Fig. 13, to further move the impedance closer to the center. Finally, the width of the slot (W_s) is adjusted to obtain wideband U-slot antenna geometry as evident from Fig. 14.

The 2:1 VSWR bandwidths of all the final, optimized U-slot antennas for the three design examples are tabulated in Table VI. The details of the optimization procedure followed to obtain wideband impedance results are discussed next.

TABLE VI
2:1 VSWR BANDWIDTHS OF PARAMETRICALLY OPTIMIZED U-SLOT ANTENNA GEOMETRIES DESIGNED VIA THE THREE EMPIRICAL TECHNIQUES FOR THE DESIGN EXAMPLES (A), (B) AND (C)

ϵ_r	method I (%)	method II (%)	method III (%)
1.0	34.21	34.29	29.47
4.0	37.58	30.56	36.81
6.15	30.20	40.39	31.54

B. Optimization via Global Optimizing Sub-Routines in `IE3D [7]`

The results of global optimization of the initial U-slot antennas designed via the three empirical techniques, are presented in Figs. 15 to 18. While, all three algorithms were used in the optimization studies, only results from Genetic and Powell optimizers are presented here.

The ability of the built-in optimizing sub-routines in IE3D, namely Genetic, Powell and Random optimizers, to rapidly optimize initial U-slot antennas, designed via method I, is discussed in [11] and is omitted here for brevity. The results presented therein indicate that the initial U-slot antennas designed via method I can be rapidly optimized via global optimizers in IE3D. The sensitivity of these optimizers to the selection of range of optimization is also documented.

In this section, the ability of the global optimizers to rapidly optimize the initial U-slot antennas, designed by methods II and III, is discussed. It must be emphasized at this point that, since IE3D is a general purpose electromagnetic simulator, the designer must

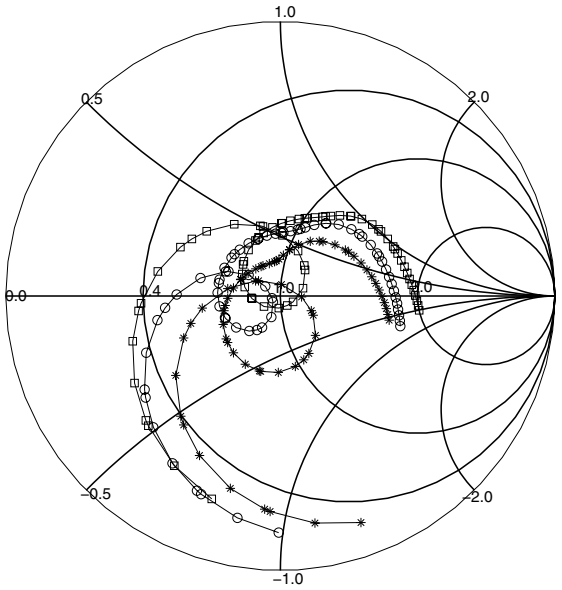

Fig. 15. Comparison of Smith Chart results of final, optimized U-slot antennas designed via method II on dielectric substrates with $\epsilon_r = 4.0$. Optimization variables - L_s and W_s; $\square - \square - \square$- parametric modeling results based optimization, $* - * - *$- after 800 generations of Genetic optimizer and $\circ - \circ - \circ -$ after 100 iterations on Powell optimizer.

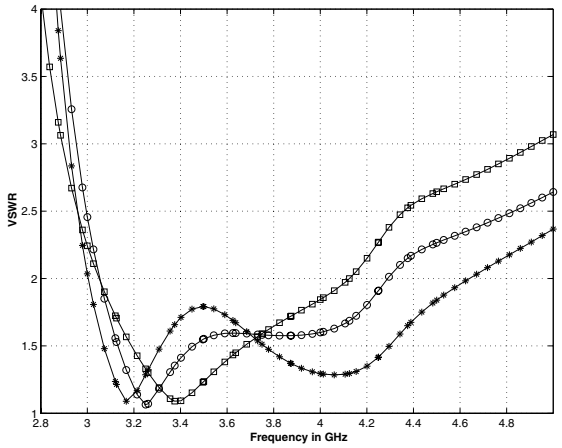

Fig. 16. Comparison of VSWR results of final, optimized U-slot antennas designed via method II on dielectric substrates with $\epsilon_r = 4.0$. Optimization variables - L_s and W_s; $\square - \square - \square$- parametric modeling results based optimization, $* - * - *$- after 800 generations of Genetic optimizer and $\circ - \circ - \circ -$ after 100 iterations on Powell optimizer.

essentially choose the optimization variables, criteria and the range over which the antenna geometry must be optimized. Here, parametric simulation results presented in [5], [9] and [10] play a vital role in selection of optimization variables for IE3D (or CAD) based optimizations.

For U-slot antenna designed via method II, both length (L_s) and width (W_s) of the slot were chosen as an optimization variable. Similarly probe location was chosen as optimization variable for U-slot antenna designed via method III. The dimensions of the final, optimized U-slot antennas, designed via methods II and III, obtained from IE3D are presented in Tables VII and VIII, respectively. The various details of the input used to set up these optimization simulations on IE3D for these optimization studies are also presented therein. The performance of the corresponding U-slot antennas, optimized via parametric modeling results, are also shown for comparison.

As seen from the figures, both Genetic and Powell optimizers on IE3D generate wideband impedance behavior in U-slot antenna geometries designed via method II. In contrast, in Figs. 17 and 18, only Powell optimizer appears to generate wideband U-slot antenna topologies for U-slot designed via method III. Overall, the results from the global optimizers in IE3D are in good agreement with the information obtained from optimization studies based on parametric modeling results in [5], [9] and [10].

TABLE VII

DIMENSIONS OF FINAL, OPTIMIZED (VIA GLOBAL OPTIMIZERS ON IE3D) U-SLOT ANTENNAS OBTAINED FOR U-SLOT ANTENNA GEOMETRY DESIGNED BY METHOD II [6], FOR DESIGN EXAMPLE (B), REFERRING TO FIG. 1. (ALL DIMENSIONS IN MM)

Parameter	Initial	Genetic Optimizer	Powell Optimizer
ϵ_r	4.0	4.0	4.0
$\tan(\delta)$	0.002	0.002	0.002
h	5.5	5.5	5.5
L	17.96	17.96	17.96
W	34.49	34.49	34.49
L_s	16.01	12.85	14.1
W_s	15.94	12.0	11.65
t	1.53	1.53	1.53
a	0.95	2.55	1.9
b	1.0	2.56	1.96
F	8.96	8.96	8.96
R_{probe}	0.635	0.635	0.635
lower freq. (f_l) in GHz	-	3.1	3.1
upper freq.(f_u) in GHz	-	4.1	4.1
Optimization variable(s)	-	L_s,W_s	L_s,W_s
Optimization criterion	-	$\lvert S_{11}\rvert \leq$ -10 dB	$\lvert S_{11}\rvert \leq$ -10 dB
Number of generations / iterations	-	800	100

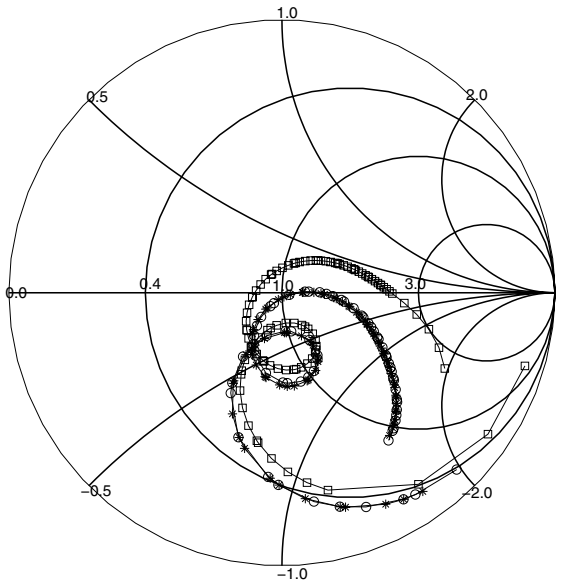

Fig. 17. Comparison of Smith Chart results of final, optimized U-slot antennas designed via method III on dielectric substrates with $\epsilon_r = 4.0$. Optimization variables - probe location; □ − □ − □- parametric modeling results based optimization, ∗ − ∗ − ∗- after 400 generations of Genetic optimizer and ○ − ○ − ○− after 100 iterations on Powell optimizer.

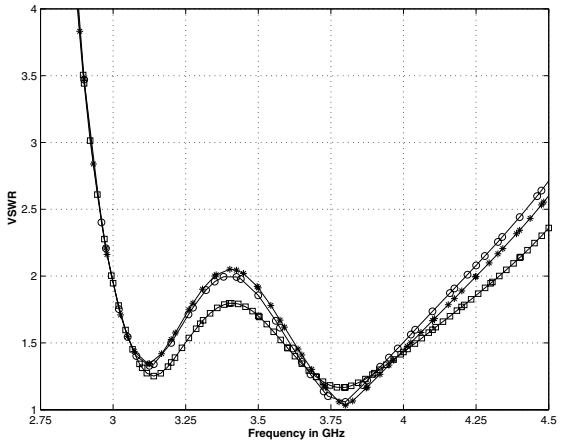

Fig. 18. Comparison of VSWR results of final, optimized U-slot antennas designed via method III on dielectric substrates with $\epsilon_r = 4.0$. Optimization variables - probe location; □ − □ − □- parametric modeling results based optimization, ∗ − ∗ − ∗- after 400 generations of Genetic optimizer and ○ − ○ − ○− after 100 iterations on Powell optimizer.

C. Comparison of Gain and Radiation Characteristics

In the previous sections of this paper, focus had been directed towards broadband characteristics of U-Slot geometries generated from the three empirical techniques, *viz.*, methods I, II and III. Return-loss and impedance data for both initial (unoptimized) and final (optimized) U-Slot designs have shown that method III, introduced in Section III of this paper, is a better choice for wideband applications of all the three empirical techniques. However for a complete performance appraisal of the three methods, it is necessary to examine other aspects of antenna performance, namely, the gain and radiation characteristics. To avoid tedium, results for gain vs. frequency and co and cross-polar radiation patterns in the $\phi = 0^\circ$ and 90° cardinal planes are included in this subsection for substrate permittivity $\epsilon_r = 4.0$ and for both initial and optimized U-Slot designs from each of the three techniques. The dimensions of the U-Slot antenna from the three techniques are available in Table IV (for both initial and optimized cases). Figs. 19 to 24 shows the relevant results, and are briefly discussed below.

In Figs. 19 and 20 the peak boresight ($\phi = 0^\circ, \theta = 0^\circ$) gain is seen to be slightly higher for designs via methods I and II, compared to method III. Interestingly, the peak gain occurs at 3.2 GHz for designs via methods II and III, while for method I the gain is at the peak around 2.8 GHz in both initial and optimized

TABLE VIII
DIMENSIONS OF FINAL, OPTIMIZED (VIA GLOBAL OPTIMIZERS ON IE3D) U-SLOT ANTENNAS OBTAINED FOR U-SLOT ANTENNA GEOMETRY DESIGNED BY METHOD III [SECTION III], FOR DESIGN EXAMPLE (B), REFERRING TO FIG. 1. (ALL DIMENSIONS IN MM)

Parameter	Initial	Genetic Optimizer	Powell Optimizer
ϵ_r	4.0	4.0	4.0
$\tan(\delta)$	0.002	0.002	0.002
h	6.45	6.45	6.45
L	18.44	18.44	18.44
W	25.54	25.54	25.54
L_s	12.76	12.76	12.76
W_s	9.93	9.93	9.93
t	1.43	1.43	1.43
a	2.84	2.84	2.84
b	2.84	2.84	2.84
F	9.22	6.57	6.445
R_{probe}	0.635	0.635	0.635
lower freq. (f_l) in GHz	-	3.0	3.0
upper freq.(f_u) in GHz	-	4.2	4.2
Optimization variable(s)	-	probe location	probe location
Optimization criterion	-	$\|S_{11}\| \leq$ -10 dB	$\|S_{11}\| \leq$ -10 dB
Number of generations / iterations	-	400	100

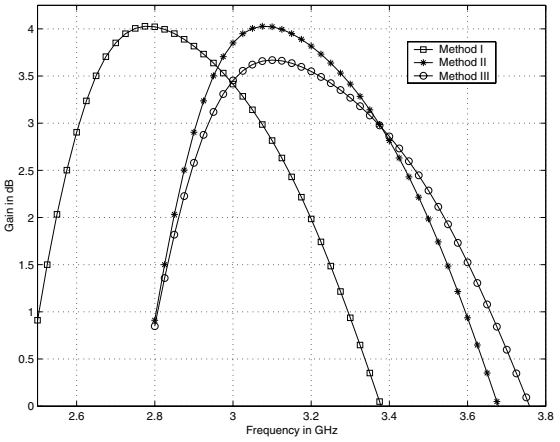

Fig. 19. Boresight gain vs. frequency for *initial* U-Slot patch designs for data in Table IV and dielectric substrates with $\epsilon_r = 4.0$

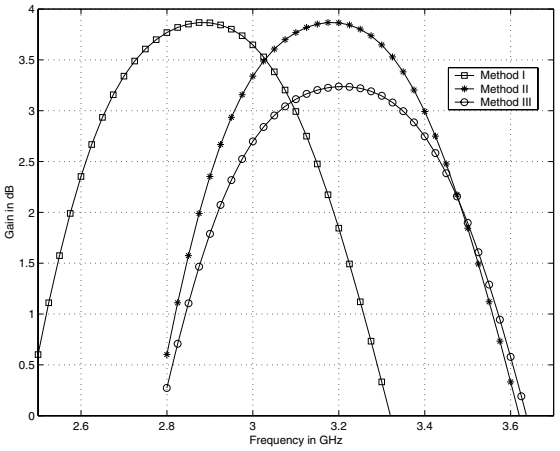

Fig. 20. Boresight gain vs. frequency for *optimized* U-Slot patch designs for data in Table IV and dielectric substrates with $\epsilon_r = 4.0$

designs.

Following the design example in [5, Section VII], empirical equations from [5, Table II] for substrate $\epsilon_r = 4.5$ were used to calculate the $\frac{\mathrm{W}}{\mathrm{h}}$ ratio for $\epsilon_r = 4.0$ at a resonant frequency of $\mathrm{f_r} = 3.2$ GHz. Subsequently the dimensional invariance relationships [5, Table I] were used to obtain the other dimensions of the U-Slot for $\epsilon_r = 4.0$. Thus, when the method I design was simulated via IE3D [7], the peak gain occured at 2.8 GHz as seen in Figs. 19 and 20. This can be realized since U-Slot dimensions obtained via method I (using empirical equations for $\epsilon_r = 4.5$) were not appropriate for $\epsilon_r = 4.0$.

One also notices in Figs. 19 and 20 the peak boresight gain differences between U-Slot designs from methods I and III are roughly 1 dB but occur at frequencies of 2.8 GHz and 3.2 GHz, respectively. The same figures also show that U-Slots designs via methods II and III have different peak boresight gains, but at the same frequency of 3.2 GHz. These features are briefly explained, below.

For U-Slots designs via methods I and III, we note from Table IV that $\frac{\mathrm{W}}{\mathrm{L}} = 1.385$ for both cases. The overall radiating (patch) area for U-slot design via method I is *larger* than that via method III. In addition, $\frac{\mathrm{h}\sqrt{\epsilon_r}}{\lambda} \approx 0.12048$ (method I at 2.8 GHz), and ≈ 0.14028 (method III at 3.2 GHz), respectively. Since the radiation efficiency, $\mathrm{e_r}$, decreases with increase in $\frac{\mathrm{h}\sqrt{\epsilon_r}}{\lambda}$ values [1, p. 288, Fig. 4.16], [2, p. 247, Fig. 5.8], it follows that the overall boresight ($\phi = 0^\circ, \theta = 0^\circ$) gain from [1, p. 277, Eq. (4.54)]

$$\mathrm{G}(\theta, \phi) = \mathrm{e_r D}(\theta, \phi). \tag{23}$$

will be larger for method I compared to method II. The same line of arugment can be extended to show that peak boresight gains for designs via methods I and II at 2.8 GHz and 3.2 GHz, respectively, will be the same as seen in Figs. 19 and 20. (We note from Table IV that the overall U-Slot patch areas via methods I and II are almost the same.)

The radiation patterns of the initial and optimzied U-Slot geometries obtained from each of the individual methods I, II and III in Figs. 21 to 24 are discussed, briefly, next.

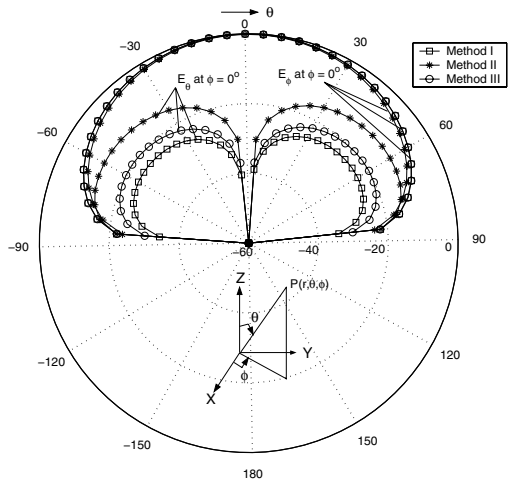

Fig. 21. Co-polar (E_ϕ) and cross-polar (E_θ) patterns for the *initial* U-Slot patch designs or data in Table IV and dielectric substrates with $\epsilon_r = 4.0$, in the cardinal plane $\Phi = 0^\circ$, at $\mathrm{f} = 3.26\mathrm{GHz}$.

The co- (E_ϕ) and cross-polar (E_θ) radiation patterns in the $\phi = 0^\circ$ principal planes are shown in Figs. 21 and 22 for the initial and optimized cases, respectively. One notices that the design via method II has the highest level of cross-polar component in comparison with the other two designs. Also, method III design has the lowest crosspolar level.

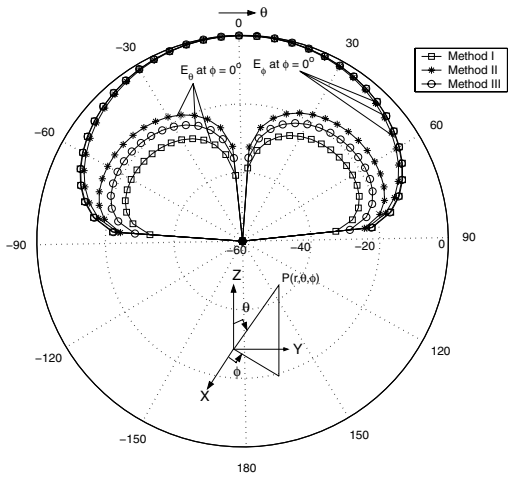

Fig. 22. Co-polar (E_ϕ) and cross-polar (E_θ) patterns for the *optimized* U-Slot patch designs or data in Table IV and dielectric substrates with $\epsilon_r = 4.0$, in the cardinal plane $\Phi = 0^\circ$ at f = 3.26GHz.

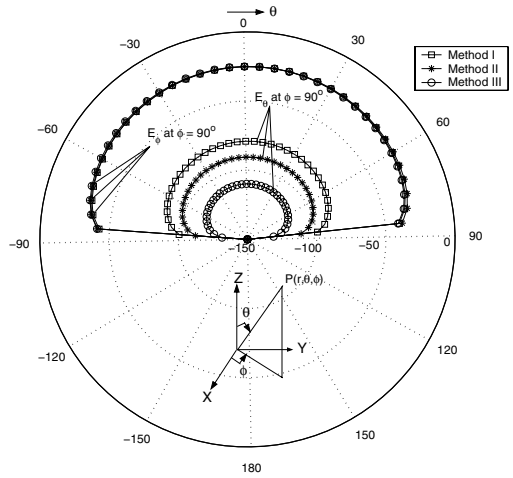

Fig. 23. Co-polar (E_ϕ) and cross-polar (E_θ) patterns for the *initial* U-Slot patch designs or data in Table IV and dielectric substrates with $\epsilon_r = 4.0$, in the cardinal plane $\Phi = 90^\circ$, at f = 3.26GHz.

One notices identical characteristics in the radiation behavior in the $\phi = 90^\circ$ principal plane as shown in Figs. 23 and 24. The crosspolar (E_θ) levels are much higher for the design via method II when compared to methods I and III.

The reasons can be traced back to the designs in Table IV. From this table, one notices that the $\frac{\mathrm{W}}{\mathrm{L}} \approx 1.385$ for the U-Slot designs via methods I and III. Quite interestingly $\frac{\mathrm{W}}{\mathrm{L}} \approx 1.98$ for the U-Slot design from method II. Since $\frac{\mathrm{W}}{\mathrm{L}} \approx 1.5$ yields a patch with lowest crosspolar power [1, p. 290, Fig. 4.17], one can conclude that the overall dimensions of a rectangular U-Slot patch via method II would yield the highest crosspolar levels as shown. In contrast for

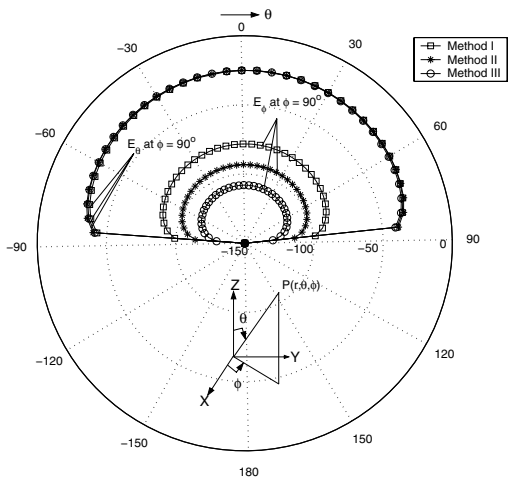

Fig. 24. Co-polar (E_ϕ) and cross-polar (E_θ) patterns for the *optimized* U-Slot patch designs or data in Table IV and dielectric substrates with $\epsilon_r = 4.0$, in the cardinal plane $\Phi = 90^\circ$ at f = 3.26GHz.

U-Slot designs via methods I and III, the crosspolar levels are comparatively smaller by roughly 10 dB.

This phenomenon was also observed for U-Slot designs on $\epsilon_r = 1.0$ and 6.15 substrate geometries. It is interesting to note that both the boresight gain and crosspolar levels could be explained fairly accurately from the corresponding characteristics of a probe-fed rectangular patch having the same overall W and L dimensions. This phenomenon suggests that the effect of the slot in the U-Slot patch is primarily to cancel the probe-inductance and produce a second resonance and contribute to the wideband characteristics.

D. Summary of Comparative Performance Analysis of Three Empirical Design Methods

In this section the main features of the three methods are summarized in Table IX.

In [5, Table II] (method I) the empirical (quadratic) curve-fit equations were developed from IE3D code [7] (method of moments) simulation results to obtain relationships of the generic form

$$\frac{\mathrm{W}}{\mathrm{h}} = \mathrm{C}_2\mathrm{f}_r^2 + \mathrm{C}_1\mathrm{f}_r + \mathrm{C}_0, \tag{24}$$

where f_r is the design (or operating) frequency in GHz. In the above, the constants, $\mathrm{C}_{2,1,0}$ need to be determined for specific substrate ϵ_r and h. Note that $\mathrm{f_r}$ is not necessarily the resonant frequency. In fact, as observed in [5], for U-Slot designs on higher ϵ_r substrates a proper resonant frequency on the Smith Chart may not strictly be found, but a minimum VSWR for a given $\mathrm{f_r}$ may still be viable. This approach, though very tedious, is in principle applicable to all classes

TABLE IX

Performance Evaluation of the Three Empirical Design Techniques

Empirical Techniques	**General Features of Initial Designs**	**Performance and Features of Optimization Approach**	
		Parametric Modeling Results [5], [9], [10]	**Global optimizers in IE3D (Genetic and Powell) [7]**
Method I [5]	(1) Initial designs, for most cases, exhibit wideband characteristics and have an overall $\frac{W}{L} \approx 1.385$. (2) Use of the empirical equations in [5, Section VI, Table II] may not always work well for all substrates, but is unique for substrates with $\frac{h\sqrt{\epsilon_r}}{\lambda} \geq 0.1$ (3) Acceptable boresight gain and cross-polar performance observed for low to high permittivity substrates	(a) Most significant control on wideband performance is exercised by a proper choice of the substrate thickness, or equivalently, the $\frac{h\sqrt{\epsilon_r}}{\lambda} \geq 0.1$ parameter. (b) Peak values of boresight gains and pattern shape remains relatively unaffected in the final optimized design (c) Readily optimized for enhanced bandwidth performance with smaller computational resources	(i) Results from parametric optmization studies agree with the global optimizers, *viz.,* Genetic and Powell algorithms in the commercial software, IE3D (ii) Other features are the same as that of parametric optimization scheme(s) for method I
Method II [6]	(4) The empirical design algorithm assumes *four distinct* resonant frequencies, although the first one is never used in the design of the U-Slot. (5) The design approach could yield negative or non-physical values for the dimension b shown in Fig. 1 for select substrate permittivities and yet the algorithm would still predict successful completion of design (6) Physically realizable designs appear viable on smaller substrate thicknesses and may not demonstrate wideband performance, compared to methods I and III (7) The initial designs have an overall $\frac{W}{L} \approx 2.0$ and have high cross-polar levels compared to methods I and III; the boresight gain is however higher than the designs via method III	(d) Parametric simulation approaches applied to the initial design from method II does indeed yield 10 dB return loss bandwidths $\geq 20\%$. (See Table VI for select performance data.) (e) Since initial designs from method II often exhibit poor bandwidths, their optimization for enhanced bandwidth performance generally requires several optimization variables over wide ranges resulting in increased demands on available computational resources. This is the *major disadvantage* of using method II. (f) Other antenna parameters such as boresight gain, radiation patterns remain largely unaffected in the final optimized design	(iii) The dimensions of the optimized U-Slot designs via global optimizers (Genetic and Powell algorithms) in the IE3D are different for the identical set of constraints. (See Table VII.) (iv) Parametric and global optimization results show acceptable agreement in performance behavior. ((See Figs. 15 and 16 for impedance and VSWR performances, respectively.) (v) Optimizing the design for bandwidth does not appear to affect the gain and radiation pattern behavior
Method III, Section III, this paper	(8) This empirical design algorithm is more verstatile and straightforward than method I, because it starts with the design of a rectangular patch that is extensively documented and well understood [1], [2]. (9) The initial design has the lowest cross-polar components of all three methods studied here. It also has the smallest boresight gain. The overall patch $\frac{W}{L} \approx 1.385$.	(g) Of all the three empirical design techniques, method III requires the least number of optimization cycles for designs exhibiting enhanced bandwidths (h) Other features were observed to be identical to (b) and (c) for method I, above	(vi) The dimensions of the optimized U-Slot designs via global optimizers (Genetic and Powell algorithms) in the IE3D are nearly identical for the identical set of constraints. (See Table VIII.) (vii) Parameric and Global optimizer results are agree very closely. (See Figs. 17 and 18 for impedance and VSWR performances, respectively.) (viii) Gain and radiation patterns remain almost unaffected in the final optimized design for enhanced bandwidths.

of substrates, and hence will work for those values of $\frac{\mathrm{h}\sqrt{\epsilon_r}}{\lambda}$ where the cavity model may not be accurate. This feature is unique only to method I and thus merits its application.

Method II is additionally constrained by the design algorithm [6] that proceeds by assuming a-priori existence of four distinct resonant frequencies of the U-Slot. As shown here, this additional assumption could sometimes result in non-physical dimensions for the U-Slot geometry. However, this apparent drawback of method II needs to be investigated in the future in more details for larger values of $\frac{\mathrm{h}\sqrt{\epsilon_r}}{\lambda}$. The present investigations found that it generated physically realizable U-Slot designs on low ϵ_r substrates with smaller h values.

Method III is versatile but is strictly restricted to substrate geometries satisfying the criterion $\frac{\mathrm{h}\sqrt{\epsilon_r}}{\lambda} \leq 0.1$ dictated by the applicability of the cavity model formulas [1], [2]. (However, for the U-Slot designs presented and studied here, method III did not show any limitations when applied to high ϵ_r substrates.) The design of the rectangular patch and its modification by the dimensional invariance technique to realize the U-Slot, appears to be the most straightforward of all the three approaches, and is free from the limitations that are intrinsic to methods I and II.

VII. Conclusion

In this investigation three empirical methods for the design of a probe-fed, U-Slot microstrip patch antennas on substrate permittivities $\epsilon_r = 1.0, 4.0,$ and 6.15 has been extensively studied for a comparative assessment of their performances. The analysis of the results from the three algorithms suggest that two of the methods (I and III), generate initial designs that exhibit superior wideband behavior. In contrast, method II was found to be limited to electrically thin and low ϵ_r substrates. Consequently, initial designs via method II have smaller bandwidths compared to other two techniques. Interestingly, the initial designs via methods I and III had lower peak cross-polar levels, when compared to method II by a factor of 10 dB. This was attributed to the fact that overall U-Slot patch dimension $\frac{\mathrm{W}}{\mathrm{L}} \approx 2.0$ (via method II). In comparison, $\frac{\mathrm{W}}{\mathrm{L}} \approx 1.385$ for U-Slot designs via I and III, which is close to the optimum value of $\frac{\mathrm{W}}{\mathrm{L}} \approx 1.5$ for a retangular patch. Therefore, methods I and III generate initial U-Slot patch designs that have good return loss bandwidths, and cross-polar performances when compared to method II.

Parametric, and global (Genetic and Powell) optimization methods were employed for further bandwidth enhancements of the three designs. The results showed that intital designs via methods I and III were rapidly optimized when compared to method II. Since method II design worked well when restricted to substrates with low $\frac{\mathrm{h}\sqrt{\epsilon_r}}{\lambda}$, its optimization for bandwidth enhancement was feasible with more (input) variables and allowing wide range parametric variations, resulting in increased computational resource requirements. The optimization process(es) did not affect the far-field (gain, radiation) behavior for all the cases studied here.

Acknowledgement

The authors thank Edwin Chettiar for generating results and careful reading of the manuscript. Thanks are due to Richard D. Swanson, Senior Staff Engineer, Honeywell FM &T, KC, MO, for his continued active interest and support. The authors gratefully acknowledge the financial support of Honeywell and the University of Missouri Research Board (UMRB) grant. It is a pleasure to acknowledge the help of Ms. Julie Burchett, Rogers Corp, Chandler, AZ for the TMM and Ultralam substrate samples. The authors also thank one of the anonymous reviewers for the suggestions that helped to improve the quality of this paper.

References

[1] R. Garg, P. Bhartia, I. Bahl and A. Ittipiboon, *Microstrip Antenna Design Handbook*. Norwood, MA, USA: Artech House, Inc., 2001.

[2] D. R. Jackson *et. al.*, "Computer-Aided Design of Rectangular Microstrip Antennas," chapter 5 in *Advances in Microstrip and Printed Antennas*, Kai-Fong Lee and Wei Chen (eds.), John-Wiley & Sons, Inc., NY, USA, 1997.

[3] K.-F. Lee, K.-M. Luk, K.-F. Tong, S.-M. Shum, T. Huynh, and R. Q. Lee, "Experimental and Simulation Studies of the Coaxially Fed U-Slot Rectangular Patch Antenna,"*IEE Proc. Microw. Antennas Propag.*, part H, vol. 144, no. 5, pp. 354-358, October 1997.

[4] K.-F. Tong, K.-M. Luk, K.-F. Lee and R. Q. Lee, "A Broad-Band *U*-Slot Rectangular Patch Antenna on a Microwave Substrate,"*IEEE Trans. Antennas Propagat.*, vol. 48, no. 6, pp. 954-960, June 2000.

[5] V. Natarajan and D. Chatterjee, "An Empirical Approach for Design of Wideband, Probe-Fed, U-Slot Microstrip Patch Antennas on Single-Layer, Infinite, Grounded Substrates,"*Applied Computational Electromagnetics Society* (ACES) *Journal*, vol. 18, no. 3, pp. 191-201, November 2003.

[6] S. Weigand, G. H. Huff, K. H. Pan and J. T. Bernhard, "Analysis and Design of Broad-Band Single-Layer Rectangular U-Slot Microstrip Patch Antennas,"*IEEE Trans. Antennas Propagat.*, vol. 51, no. 3, pp. 457-468, March 2003.

[7] Zeland Software, Inc., *IE3D User's Manual*, Release(s) 9.0. Fremont, CA, USA.

[8] V. Natarajan, E. Chettiar, and D. Chatterjee, "Performance of Two Empirical Techniques for Design of Optimized, Wideband, U-Slot Antennas," *IEEE Antennas and Propagation and* URSI/USNC *Symposium Digest*, vol. 3, pp. 2424-2427, Monterey, CA, June, 2004.

[9] E. Chettiar, V. Natarajan, and D. Chatterjee, "Effect of Slot Width Variation on Performance of Wideband, Probe-Fed, U-slot Patch Antennas,"*IEEE Antennas and Propagation and* URSI/USNC *Symposium Digest*, vol. 2, pp. 1792-1795, Monterey, CA, June, 2004.

[10] V. Natarajan and D. Chatterjee, "An Empirical Design Technique for U-slot Microstrip Antennas on Microwave Substrates; Part-I: Infinite Ground Plane Analysis," technical report ECE-UMKC02-HNYWL-TR01, prepared under contract for Honeywell Federal Manufactoring and Technologies, KC, MO, ECE Division, SICE, UMKC, September 2002.

[11] V. Natarajan and D. Chatterjee, "Optimization Studies for Single-Layer, Wideband, U-Slot Antennas on Microwave Substrates Using the IE3D Code," *Proceedings of 20^{th} Annual Review of Progress in Applied Computational Electromagnetics* at Syracuse, NY, April 19-23, 2004.

[12] V. Natarajan and D. Chatterjee, "Effect of Substrate Permittivity and Thickness on Performance of Single-Layer, Wideband, U-Slot Antennas on Microwave Substrates," *Proceedings of 20^{th} Annual Review of Progress in Applied Computational Electromagnetics* at Syracuse, NY, April 19-23, 2004.

[13] R. Bhalla and L. Shafai, "Resonance Behavior of Single U-Slot Microstrip Patch Antennas," *Microwave and Optical Technology Letters*, vol. 32, no. 5, pp. 333-335, March 5 2002.

[14] E. Chettiar, V. Natarajan, and D. Chatterjee, "Comparison of Resonant Frequency Calculations for Wideband U-Slot Antennas on Microwave Substrates," *IEEE Antennas and Propagation and* URSI/USNC *Symposium Digest*, vol. 4, pp. 3713-3716, Monterey, CA, June 21-27, 2004.

[15] D. Chatterjee, "Development of a Fast, Iterative Computer Code for Simulations of Probe-Fed, Rectangular Patch Microstrip Antennas," part II of report ECE-UMKC00-HNYWL-TR01, June 2000, prepared under contract for Honeywell International Inc., FM&T, KC, MO.

Venkataraman Natarajan was born in Chennai, India on July 2, 1978. He received his M.S. and B.S. degrees in Electrical Engineering from the University of Missouri-Columbia, USA, and University of Madras, Chennai, India, in 2002 and 2000, respectively. Since August 2000 he has been working as a Graduate Research Assistant at the Computational Electromagnetics Laboratory at the University of Missouri Kansas City. He was awarded the Outstanding Graduate Student award in April 2001. He has been an IEEE Student Member since August 1998. Mr. Natarajan is currently working as a technical consultant at Seattle, WA.

Deb Chatterjee received B.E.Tel.E (Bachelor's) degree in Electronics and Telecommunication Engineering from Jadavpur University, Kolkata (Calcutta), India, in 1981, M.Tech (Master's) degree in Electronics and Electrical Communication Engineering from IIT Kharagpur, India, in 1983, M.A.Sc (Master of Applied Science) degree in Electrical and Computer Engineering from Concordia University, Montreál, Canada, in 1992, and, the Ph.D. degree in Electrical Engineering from the Department of Electrical Engineering and Computer Science, University of Kansas, Lawrence, USA in 1998. From 1983-1986 he worked with the Antenna Group at Hindustan Aeronautics Limited (HAL), Hyderabad, India, on monopulse feeds for applications to the Fire Control Radar. Since August 1999 he is an Assistant Professor with the Electrical and Computer Engineering, University of Missouri Kansas City (UMKC). His current research interests are, analytical and numerical techniques in electromagnetics - with an emphasis on (asymptotic) high-frequency applications, modeling of planar and conformal phased and smart antenna arrays, analysis and design of wideband microstrip antenna elements, and, electromagnetic effects in biological systems. Dr. Chatterjee is a member of the IEEE Antennas and Propagation and Applied Computational Electromagnetics Societies, and has served as a technical reviewer for the *IEEE Transactions on Antennas and Propagation*, *IEEE Antennas and Wireless Propagation Letters*, *IEEE Transactions on Vehicular Technology*, *Applied Computational Electromagnetics Society Journal*, and *Radio Science*. He has also served as a summer technical consultant to Honeywell Federal Manafacturing and Technologies, KC, MO.